ISSN 2029-6991 / eISSN 2029-7009

VILNIUS TECH
Vilnius Gediminas Technical University

GEODESY and CARTOGRAPHY

2026
Volume 52
Issue 2
Pages 55–65
https://doi.org/10.3846/gac.2026.22770

UDC 528.7: 528.48: 622.1

COMPARISON OF UNMANNED AERIAL VEHICLE (UAV) AND DEMNAS IN LANDSLIDE MAPPING IN THE LEMBANG FAULT AREA, INDONESIA

Nanin Trianawati SUGITO ✉, Haikal Muhammad IHSAN, Shafira HIMAYAH, Asri Ria AFFRIANI, Anisa Nabila Rizki RAMADHANI

Faculty of Social Sciences Education, Universitas Pendidikan Indonesia, Bandung, Indonesia

Article History:
- received 27 November 2024
- accepted 5 May 2026

Abstract. The Lembang Fault area has a high potential for landslides due to its location in an active structural zone that shifts annually. The fault movement causes ground displacement, making it important to study landslide potential. Unmanned Aerial Vehicle (UAV) technology can produce Digital Terrain Model (DTM) products with a spatial resolution of 6 cm. This study aims to compare DTM and DEMNAS products in landslide mapping within the Lembang Fault area, West Java Province, Indonesia. The method employed in this research is the Analytic Hierarchy Process (AHP) with variables including slope, aspect, curvature, lineament density, drainage density, Topographic Wetness Index (TWI), rainfall, and lithology. The analysis results show that the Root Mean Square Error (RMSE) of the DTM product is 0.902, indicating that the UAV data acquisition provides better accuracy in landslide mapping compared to the DEMNAS product with an RMSE of 1.592. Although the landslide maps produced from DTM and DEMNAS share similar patterns, the area classifications differ due to their varying spatial resolutions. Both products are equally effective in mapping landslides in the Lembang Fault area, as they both exhibit good RMSE values in the analysis.

Keywords: Unmanned Aerial Vehicle (UAV), DEMNAS, landslide, Digital Terrain Model (DTM).

✉Corresponding author. E-mail: ***nanintrianawati@upi.edu***

1. Introduction

In geology, a fault refers to a fracture plane where there is relative movement between two rock blocks. Faults typically form when rocks are subjected to forces, such as compression, tension, or a combination of both, which exceed the rock's ability to resist, leading to displacement (Ricky & Basyid, 2021). Landslides commonly occur in mountainous or elevated areas. With the use of modern Geographic Information System (GIS) and remote sensing technologies, it is possible to assess and map slope hazards across a given region. GIS is a computer-based tool designed for collecting, storing, capturing, analyzing, and displaying data (Ya'acob et al., 2024). Landslides are a frequent geological hazard in fault zones, where active faults can greatly impact land stability. These areas are often linked to seismic activity, ground shifts, and unstable terrain, all of which heighten the risk of landslides. Such landslides may result directly from earthquakes or from the gradual weakening of the landscape in regions prone to faults.

The Lembang Fault is located about 10 km north of the city of Bandung and extends in a west – east direction through the city of Lembang. The level of activity of the Lembang Fault is not yet well known, so more integrated research is needed using several methods, including seismic methods, gravity methods and deformation methods (Rasmid, 2014). This fault zone is distinctly recognizable as a prominent feature where the slope breaks between a series of east-west-aligned linear ridges. These ridges separate the elevated northern Bandung highlands from the broad, flat Lembang basin located further to the north (Daryono et al., 2019).

The Lembang Fault, situated in West Java, Indonesia, is a prominent active fault zone, and mapping this fault is essential for assessing seismic risks in the area. The Lembang Fault is considered an active fault, meaning it has experienced movement in recent geological time and has the potential to produce significant seismic events. Many studies have explored the fault to investigate its geological characteristics, seismic activity, and potential to trigger

earthquakes and landslides (Shao & Xu, 2022). A Digital Elevation Model (DEM) is a crucial tool for landslide mapping, providing detailed topographical information that helps in identifying areas prone to landslides (Saleem et al., 2019). DEMs represent the Earth's surface in a 3D format by capturing elevation data, enabling the analysis of slope angles, terrain features, and watershed areas, all of which are important for assessing landslide susceptibility (Qiu et al., 2022). By analyzing elevation variations, researchers can identify steep slopes, potential landslide paths, and areas where water accumulation might destabilize the terrain.

DEM-based analysis can also be combined with other geospatial data, such as soil type, vegetation cover, and rainfall patterns, to create more accurate landslide hazard maps. Advanced techniques, like slope stability models and Geographic Information System (GIS) tools, often rely on DEMs to predict landslide risks (Zhao et al., 2017) and aid in disaster management planning. One available DEM dataset is the National Digital Elevation Model (DEMNAS) developed by the Geospatial Information Agency (BIG). DEMNAS is generated from multiple data sources, including IFSAR, TERRASAR-X, and ALOS PALSAR, supplemented by mass point data from stereo-plotting. DEMNAS can be access through (https://tanahair.indonesia.go.id/portal-web/unduh) freely. It has a spatial resolution of 0.27 arcseconds and utilizes the EGM2008 vertical datum (Tjahjadi et al., 2020).

Landslide mapping using UAVs or drones is an effective method for quickly and accurately identifying and mapping landslide-prone areas. With UAV technology, difficult-to-access regions or steep terrains can be easily surveyed without posing safety risks to the survey team (Lindner et al., 2016). UAVs are equipped with high-resolution cameras, enabling the capture of highly detailed imagery for landslide mapping (Eker et al., 2018). These images are then processed using photogrammetry software to produce high-resolution orthophoto models of the ground surface (Sun et al., 2024). This process is highly beneficial for monitoring ground surface changes in landslide-prone areas and for more efficient disaster risk mitigation planning.

UAV data can also be transformed into Digital Terrain Models (DTMs), which are crucial for landslide mapping analysis. DTMs provide a digital representation of the Earth's surface by filtering out objects like vegetation and buildings, revealing only the natural terrain contours (Artese & Perrelli, 2018). By combining DTM products with UAV data, experts can precisely identify slope gradients, drainage patterns, and areas of ground displacement. This data is essential for slope stability analysis and predicting future landslide risks (Conforti et al., 2020). The results of such mapping support informed mitigation strategies, such as identifying safe zones, constructing landslide barriers, or reinforcing vegetation on vulnerable slopes.

Non-contact remote sensing techniques, such as Unmanned Aerial Vehicle (UAV) photogrammetry, have been globally applied for landslide monitoring in high and steep mountainous areas. Mapping using UAV have advantages including: Inexpensive microdrones; On-site ground control points (GCPs) required; and Route flexibility (Zhou et al., 2023). Based on the background that has been explained, this research aims to. Map the Lembang fault area using UAV, Analyze the potential for landslides on the Lembang Fault using spatial modeling, and compare the height of UAV data products with DEMNAS for landslide mapping. The novelty of this research lies in the spatial comparative evaluation between an ultra-high-resolution UAV-derived DTM and a national elevation dataset (DEMNAS) to map landslide hazards along the geologically complex Lembang Fault. Through this approach, the study establishes a critical scientific benchmark regarding the impact of spatial resolution on geological disaster modeling, providing essential guidance for data selection in local disaster mitigation strategies.

2. Methods

This research was conducted in the Lembang Fault corridor area, specifically in the central segment. The mapped fault spans 12.33 km in length, with the research area encompassing a 1 km buffer zone around the central segment of the Lembang Fault, covering a total area of 2,685.53 hectares (Figure 1). This location is an active fault zone, making it prone to landslide disasters. Several locations within the area have residential land cover, which poses a high risk to these settlements in the event of a landslide. The study utilized a Digital Terrain Model (DTM) acquired from UAV data with a Ground Sampling Distance (GSD) of 6 cm and the DEMNAS product, which has a spatial resolution of 0.47 arcseconds.

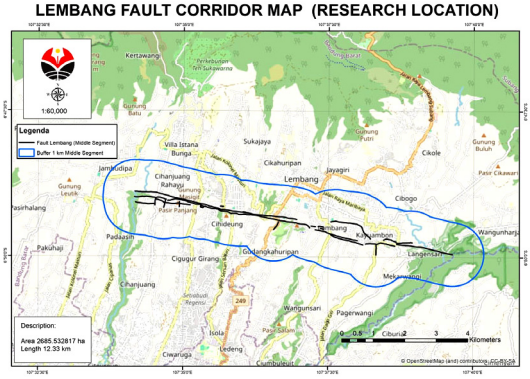

Figure 1. Research area

2.1. Lineament density

Lineaments density (distance from linear features such as faults, faults, or geological cracks) has a significant influence on landslide risk, because lineaments are areas of structural weakness in rocks or soil. Slopes that are close to lineaments tend to be more susceptible to landslides, due to the potential for ground movement or cracks that affect slope stability (Sadiq et al., 2022). Active faults or faults can cause sudden ground movement (Hussin et al.,

2022), while other cracks or lineaments can be pathways for water infiltration, which increases pore water pressure and weakens the strength of the surrounding soil (Abduh et al., 2021). The closer an area is to a lineament, the more likely the slope is to experience landslides, especially when heavy rainfall or tectonic activity occurs (Mathew et al., 2007). Lineament density was analyzed using GIS software, with the following equation:

$$LD = \frac{\sum_{i=1}^{i=n} Li}{A}. \quad (1)$$

The above equation describes that the *LD* is, *Li* is the total length of lineament, whereas *A* is the width of the studied area.

2.2. Drainage density

Drainage density is closely related to landslide risk, because it shows how intensive the water flow system is in an area. Areas with high drainage density have a dense water flow network, which means more water flows through the soil and slope surface (Pradhan & Kim, 2018). This can lead to increased soil erosion and erosion of materials on the slope, thereby reducing its stability (Chauhan et al., 2010). In addition, high drainage density increases infiltration and water saturation on the slope, which can increase pore water pressure and weaken the shear strength of the soil, making it more susceptible to landslides, especially during high rainfall (Rai et al., 2014). Conversely, areas with low drainage density tend to have a lower risk of landslides, because there is less water flow and the soil can absorb water better. Drainage density is an important indicator in landslide risk analysis and slope vulnerability mapping (Arrasyid et al., 2023). Drainage density can be calculated using the following equation Horton (1932):

$$d = \sum_{i=1}^{n} Di / A\left(\mathrm{km}^2\right). \quad (2)$$

The equation describes that *d* is the river density (km/km^2), *Di* is the whole length of the river (km^2), and the identification coverage.

2.3. Slope

Slope or slope gradient has a direct relationship with the potential for landslides, because steep slopes increase the risk of soil instability. Slopes with high slopes (steep) tend to have a greater gravitational force that pulls slope material down, increasing the chances of landslides (Çellek, 2020), especially if the soil composition is not dense or there is a high-water content due to heavy rain (Zou et al., 2021). When the slope reaches a critical point where the frictional force and soil strength are no longer able to withstand the force of gravity, the slope can collapse, causing landslides (Intrieri et al., 2019). Therefore, slope monitoring and land management in areas with high slopes are very important to prevent landslide disasters (Li & Mo, 2019).

2.4. Curvature

Curvature plays an important role in determining the susceptibility of a slope to landslides, because it affects the pattern of water flow and the distribution of earth pressure. Curvature is divided into two main types: concave curvature and convex curvature (Sun et al., 2020). Slopes with concave curvature tend to collect water and sediment, thereby increasing the pore water pressure in the soil and adding load to the slope, which can trigger landslides if the slope is unstable (Samia et al., 2017). Slopes with convex curvature tend to be more stable because water flows more easily and is not retained, but these areas are still at risk of landslides if the material on the slope surface is eroded or dislodged (Neamat & Karimi, 2020).

2.5. Rainfall

Rain has a strong relationship with landslides, because high rainfall can affect soil conditions and slope stability. When it rains, water seeps into the soil, and if the amount of rainfall exceeds the infiltration capacity of the soil, saturated conditions will be created (Segoni et al., 2018). In this state, the pore water pressure in the soil increases, reducing the cohesion and shear strength of the soil, which in turn increases the risk of landslides. In addition, intense rain can cause surface erosion, which erodes the soil layer that supports the slope, as well as triggering water flows that can damage the soil structure (Ran et al., 2018). The type of soil also has an influence, where clay (Roccati et al., 2021), for example, can expand when wet and shrink when dry, causing instability (Meneses et al., 2019).

2.6. Topographic Wetness Index (TWI)

Topographic Wetness Index (TWI) is closely related to landslide risk, because this index indicates the potential for water accumulation in an area based on topography. TWI measures how wet a location is by considering the slope gradient and the area of water flow contribution (Różycka et al., 2017). Areas with high TWI values tend to have greater water accumulation, which can increase pore water pressure in the soil. This condition can weaken the shear strength of the soil, making the slope more susceptible to movement and landslides, especially during high rainfall (Jancewicz et al., 2019). Conversely, areas with low TWI tend to be drier and more stable, with a lower risk of landslides. TWI is an important indicator in landslide susceptibility analysis, because it provides information on the potential for water saturation and soil moisture that affect slope stability (Sujit, 2015). The TWI uses the following calculation below:

$$\mathrm{TWI} = ln\left(\frac{\alpha}{\tan\beta}\right). \quad (3)$$

The equation describes that α is the area of the non-slope contributing site and β is the slope angle. The study of TWI was analyzed using the SAGA GIS software.

2.7. Aspect

Aspect (slope direction) affects the vulnerability of a slope to landslides because it determines the slope's exposure to environmental factors such as sunlight, wind, and rain (He et al., 2024). Slopes facing a certain direction, for example towards the dominant wind or high rainfall, tend to experience erosion and water saturation more quickly, which can reduce soil strength and increase the risk of landslides (Capitani et al., 2013). In addition, aspect also affects soil temperature and humidity, where slopes facing the sun (usually slopes facing north in the southern hemisphere and south in the northern hemisphere) tend to be drier and less stable than shaded slopes (Gorokhovich & Vustianiuk, 2021). Aspect is one of the important parameters in predicting and analyzing landslide potential, because it affects the physical conditions and humidity that determine slope stability (Pawłuszek et al., 2019).

2.8. Lithology

Lithology (the type and characteristics of rocks or soil in an area) greatly affects landslide susceptibility, because the physical and mechanical properties of each type of rock or soil differ in terms of strength and stability (Henriques et al., 2015). Soft rocks, such as clay or weathered rocks, tend to be more susceptible to weathering, erosion, and softening when exposed to water, making them more susceptible to landslides. Meanwhile, hard and compact rocks, such as granite or dense sandstone, are usually more stable and have a lower risk of landslides, unless there are cracks or faults (Sulaiman et al., 2019). In addition, soil types such as clay can absorb water quickly and expand, which increases pore water pressure and makes slopes more susceptible to landslides (Roda-Boluda et al., 2018).

2.9. Analytical Hierarchy Process (AHP)

This Research using Analytic Hierarchy Process (AHP) in the context of landslides aims to systematically identify and analyze various factors that contribute to landslides. Criteria such as slope, aspect, curvature, landuse, drainage density, lineament distance, Topographic Wetness Index, lithology, and rainfall are identified and arranged in a hierarchical structure. Through assessment and comparison between criteria using a numerical scale, relative weights are calculated for each criterion, reflecting its contribution to landslides. The following is a table of AHP calculations. The formula of the consistency index is the following:

$$CI = \frac{\lambda \max - n}{n-1}; \quad CR = \frac{CI}{RI}. \tag{4}$$

The equation describes *CI* as the consistency index, *CR* as the consistency ratio, and n as the number of variables. *RI* is the Random Consistency Index obtained from the matrix table (Table 1).

Table 1. AHP calculation

No	Variable	Score	Weight
1	Slope	(0.22), (0.44), (0.66), (0.88), (1)	0.888
2	Aspect	(0.22), (0.44), (0.66), (0.88), (1)	0.333
3	Curvature	(0.22), (0.44), (0.66), (0.88), (1)	0.222
5	Drainage Density	(0.22), (0.44), (0.66), (0.88), (1)	0.555
6	Lineament density	(0.22), (0.44), (0.66), (0.88), (1)	0.777
7	Topographic wetness index	(0.22), (0.44), (0.66), (0.88), (1)	0.111
8	Lithology	(0.22), (0.44), (0.66), (0.88), (1)	0.444
9	Rainfall	(0.22), (0.44), (0.66), (0.88), (1)	0.666

The landslide results will be validated using the RMSE equation which will be compared with the results of landslide distribution in the field.

$$RMSE = \pm\sqrt{\frac{1}{n}\sum_{i=1}^{n}\left[\left(x_i - y_i\right)^2\right]}; \tag{5}$$

$$STDEV = \sqrt{\frac{1}{n-1}\sum_{i=1}^{n}\left[\left(x_i - y_i\right) - \left(\bar{x} - \bar{y}\right)\right]^2}, \tag{6}$$

where: *RMSE* – Root mean square error; *STDEV* – Standard deviation; *N* – The number of GCPs; x_i – DEM elevation at the referenced point *i*; y_i – DEM elevation at the point *i*; $\bar{x}$ – DEM elevation at the referenced point I; $\bar{y}$ – DEM elevation at the point i.

3. Results

3.1. Lineament density

Lineaments in the context of this study refer to linear features captured in elevation products, including both DTM and DEMNAS. The extracted lineaments may represent areas where valleys and ridges intersect, which could indicate the presence of local faults. The results of lineament density extraction from DTM and DEMNAS show slight differences in patterns, but these differences are not significant. The lineaments extracted from DTM are very detailed, resulting in shorter and more widely distributed features. In contrast, DEMNAS produces moderately sized lineaments that are concentrated in specific locations with clear linear indications.

The lineament density results from DTM reveal that the highest density values are located in the eastern and western areas of the Lembang Fault. On the other hand, DEMNAS shows that lineament density distribution tends to be concentrated in the western area, while the eastern area spreads toward the northeast. The extracted values for lineament density in DTM range from 0 to 13.06 ha (Figure 2), whereas DEMNAS shows density values ranging from 0 to 931.47 ha (Figure 3).

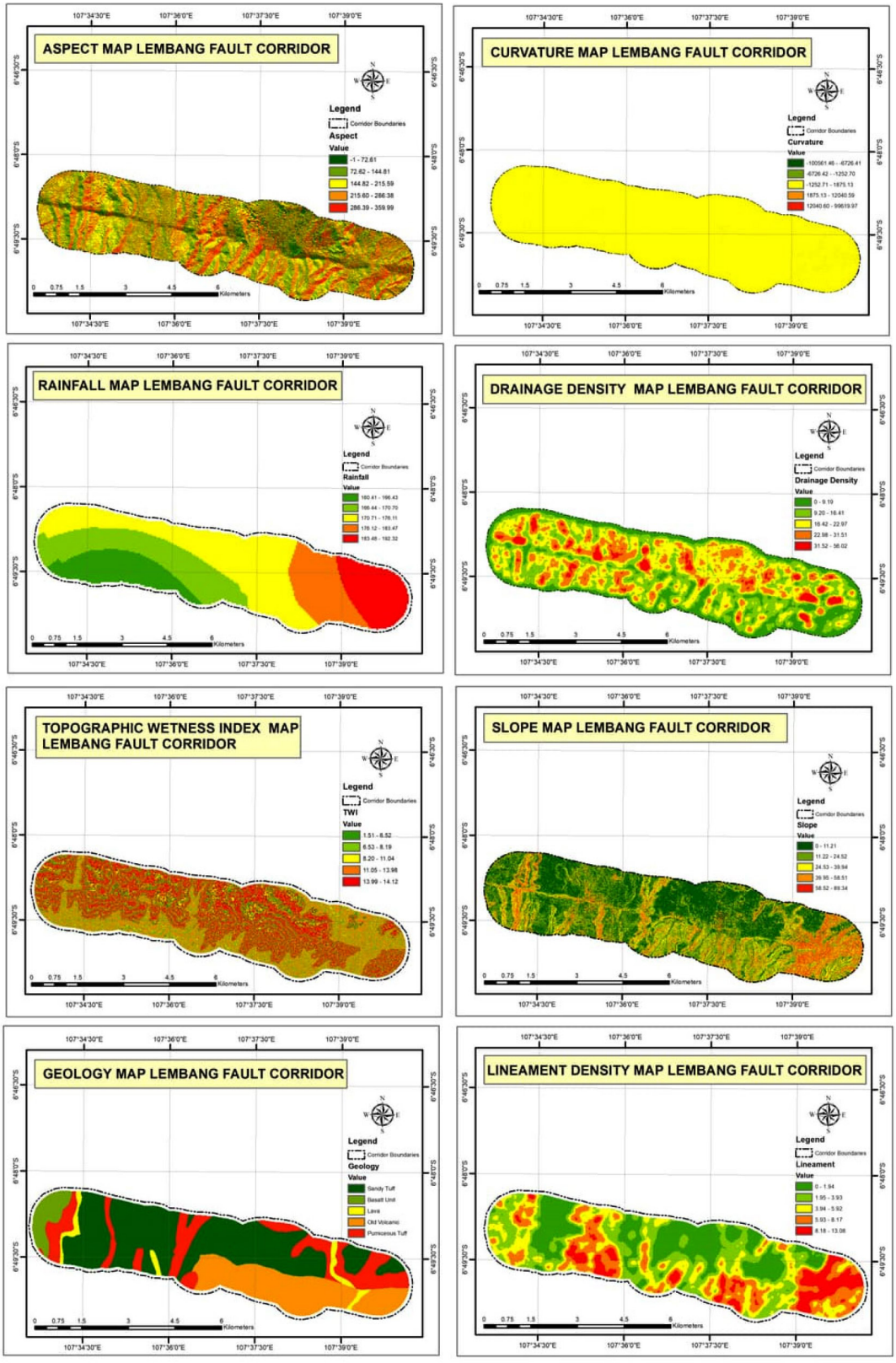

Figure 2. Landslide parameters of the Digital Terrain Model (DTM) product

3.2. Drainage density

The drainage density in DTM and DEMNAS products exhibits a similar pattern, but DTM provides more detailed assessments of density compared to DEMNAS. This is reflected in the number of river orders extracted from the elevation data. The number of river orders in DTM products is higher than those in DEMNAS products, allowing for a more visible depiction of river branching, from the largest rivers to the smallest ones, including intermittent streams.

Visually, DTM products show a higher number of areas with dense drainage compared to DEMNAS, owing to the greater number of river orders or branches, making DTM highly suitable for drainage density analysis. The extracted drainage density values from DTM range from 0 to 56.02 ha (Figure 2), whereas DEMNAS values range from 0 to 931.47 ha (Figure 3). The density values are distributed across nearly the entire Lembang Fault area, with the majority concentrated in the northern region. In the central part of the area, drainage density values change significantly, a condition likely caused by the presence of a structural feature extending through the central region.

3.3. Slope

DEMNAS and DTM products have significantly different spatial resolutions based on their respective value units. The slope pattern exhibits similar spatial distribution, but the specific values differ. DTM illustrates slopes in greater detail for each pixel value, resulting in slope values that differ from those visualized by DEMNAS, which has a medium spatial resolution.

The slope values in DTM products are categorized as follows: very low (0–11.21), low (11.22–24.52), medium (24.53–39.94), high (39.95–58.51), and very high (58.52–89.34) (Figure 2). Meanwhile, DEMNAS products exhibit smaller slope value ranges: very low (0–7.54), low (7.55–14.36), medium (14.37–21.54), high (21.55–30.11), and very high (30.12–59.06) (Figure 3).

Based on the results from both elevation products, very steep slopes are predominantly located in the eastern area of the Lembang Fault, which consists of mountainous and hilly regions. Very steep slopes are also observed along rivers with high-gradient banks, forming ridges. These areas are often associated with lahar (volcanic mudflow) paths. In the western segment of the Lembang Fault, steep slopes are also found and are relatively dominant in certain locations.

3.4. Curvature

The curvature values extracted from DTM and DEMNAS products show significant differences. The smaller the spatial resolution of a DEM product, the more varied the curvature values become, including both concave and convex curvatures. The curvature values in the DTM product are very large, ranging from –100,561.46 to 99,619.97, whereas DEMNAS values are more normalized, ranging from –29.959 to 23.959 (Figure 2).

The spatial resolution of DTM is highly detailed, down to the centimeter scale, allowing the curvature algorithm to interpret even the smallest slopes comprehensively, which may result in identifying values that do not represent actual slope curvature. This condition is explained by the spatial distribution of curvature in DTM, where noticeable values are limited to a medium range of –1,252.71 to 1,875.13. High-resolution curvature products require further correction or upscaling to normalize the curvature values. In contrast, the curvature values in DEMNAS tend to be normalized, and the spatial distribution clearly illustrates significant slope breaks (Figure 3).

3.5. Rainfall

Rainfall conditions in the Lembang Fault area tend to exhibit high intensity. The Lembang Fault is located at elevations close to several mountains, making orographic rain highly likely in the region. Based on the analysis of average monthly rainfall, the values range from 160.41 mm/month to 192 mm/month (Figures 2–3).

The rainfall data is divided into five segments according to the existing conditions of the area. The highest rainfall values are found in the eastern part of the Lembang Fault. This area features dense, pristine vegetation and is located near several mountains, such as Mount Bukit Tunggul, Mount Sanggara, and others, resulting in higher orographic rainfall compared to surrounding areas. In contrast, the lowest rainfall values in the Lembang Fault area are observed in the southwest, which consists of urban areas with relatively dense settlements.

3.6. Topographic Wetness Index (TWI)

The TWI (Topographic Wetness Index) analysis using DEMNAS data tends to show a well-distributed pattern. In this study, TWI values are based on the DEMNAS product. The DTM product exhibits a similar pattern to DEMNAS, differing only in pixel size for the extracted TWI values. The extracted TWI values range from 1.51 to 14.12, divided into five classifications according to the existing conditions in the study area.

The classifications are as follows: very low (1.51–6.52), low (6.53–8.19), medium (8.20–11.04), high (11.05–13.96), and very high (13.99–14.12) (Figure 2). Spatially, low TWI values are predominantly found in the eastern and southern areas, characterized by variable hilly terrain. Meanwhile, high TWI values are mostly concentrated in the northern part of the Lembang Fault (Figure 3). The Lembang Fault area is highly suitable for Topographic Wetness Index analysis due to its varied morphological conditions.

3.7. Aspect

The aspect values in both DTM and DEMNAS products are identical, ranging from –1 to 359.99. Aspect values are generally universal and consistent regardless of the elevation product used for analysis. The aspect values from both products are classified into five categories (Figure 2):

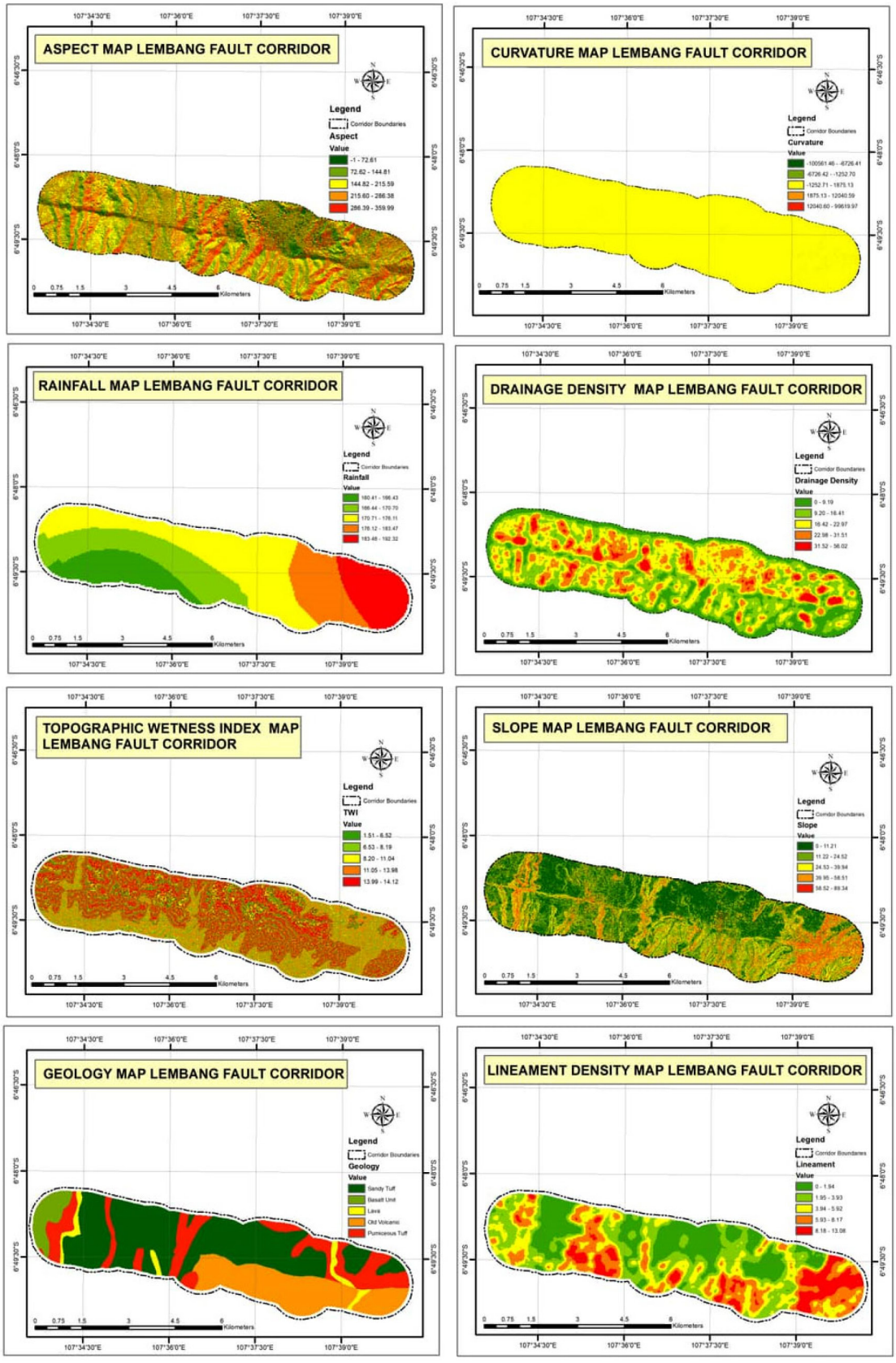

Figure 3. Landslide parameters of the DEMNAS product

- Flat, North, Northeast, and part of East: –1 to 72.61
- Part of East, Southeast, and part of South: 72.62 to 144.81
- Part of South and part of Southwest: 144.82 to 215.59
- West: 215.60 to 286.38
- Northwest and North: 286.39 to 359.99.

The aspect analysis results show a similar pattern between the two products, both DTM and DEMNAS (Figure 3). Both products tend to remain consistent according to their spatial resolutions, with DTM providing a clearer and sharper representation compared to DEMNAS.

3.8. Lithology

The geology of the Lembang Fault area dates back to the Pleistocene epoch, part of the Quaternary period approximately 2.5 million to 11,700 years ago. Generally, the Lembang Fault area is volcanic due to its close proximity to the active volcano Mount Tangkuban Parahu. According to the geological map, the parent materials in the Lembang Fault area include sandy tuff, lava, old volcanic formations, and pumiceous tuff (Figure 3).

Sandy tuff is the most widespread parent material, predominantly located in the central area of the Lembang Fault, spreading from east to west. Pumiceous tuff is scattered in several locations, particularly in valleys, ridges, and hilly areas (Figure 2). Lava is found only in a few spots, mainly along lahar paths originating from Mount Tangkuban Parahu. Old volcanic formations are evenly distributed in the southeastern area. This parent material is presumed to be remnants of ancient eruptions from the prehistoric Sunda Volcano, which has evolved into the present-day Mount Tangkuban Parahu.

3.9. Landslide

Based on the analysis of DTM and DEMNAS products, landslides in the Lembang Fault area are predominantly distributed in the western region, while the lowest occurrences are scattered in parts of the northern and western regions. Spatially, the landslide distribution patterns derived from DTM and DEMNAS are similar; however, differences in spatial resolution result in varying representations for certain classifications (Figure 4).

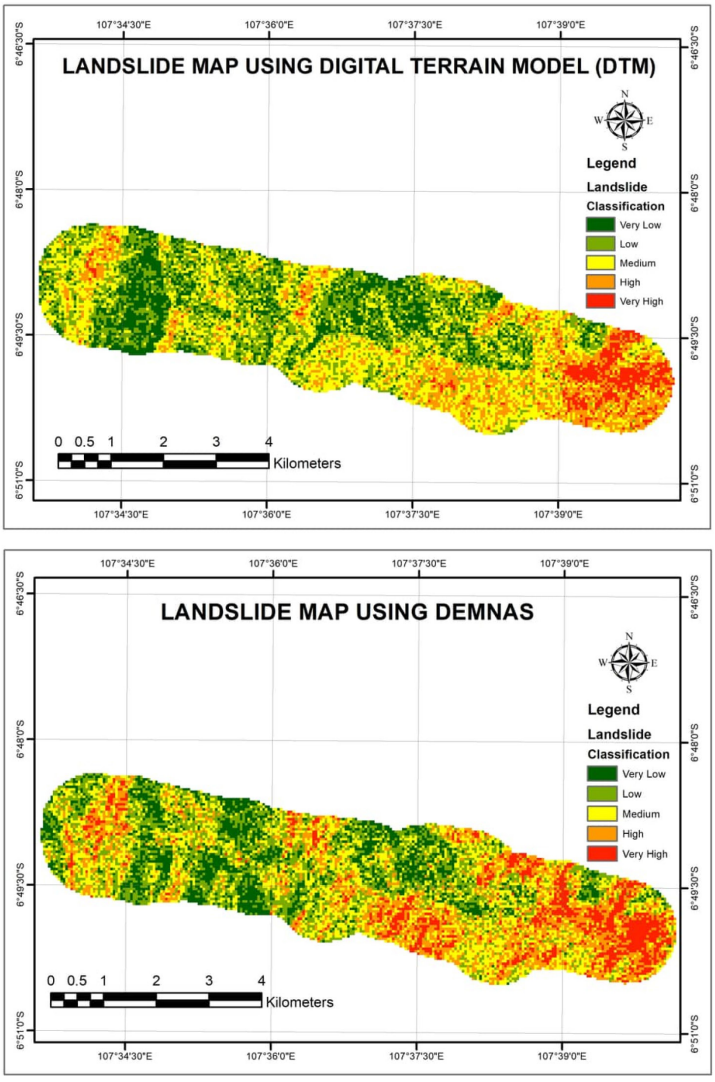

Figure 4. Landslide DTM and DEMNAS product

The landslide susceptibility is divided into five classifications: very high, high, medium, low, and very low. A comparison of area proportions shows that the "very high", "high", and "medium" classes have almost similar proportions. However, for the "low" and "very low" classes, the area proportions of DTM and DEMNAS products differ significantly (Table 2).

In general, the Lembang Fault area is a landslide hazard zone, as evidenced by the substantial area covered by the "very high", "high", and "medium" classifications. A comparison of RMSE (Root Mean Square Error) values between the two products indicates that DTM, with an RMSE of 0.902, is more accurate than DEMNAS, which has an RMSE of 1.592 (Table 3).

These findings suggest that DTM, derived from UAV data acquisition, provides better accuracy for landslide mapping compared to DEMNAS. This implies that the smaller the spatial resolution, the better the quality of landslide susceptibility mapping.

Table 2. Landslide area based on classification

No	Landslide clasification	DTM (ha)	DEMNAS (ha)
1	Very high	471.36	427.17
2	High	687.28	649.44
3	Medium	894.36	731.71
4	Low	450.51	549.46
5	Very low	147.62	300.12

Table 3. RMSE value landslide

No	DTM	DEMNAS	RMSE DTM	RMSE DEMNAS
1	High	High	0.8528029	1.3142575
2	Very high	Very high	0.8366600	1.3416408
3	High	High	0.8819171	1.4142136
4	Very high	Very high	0.8660254	1.4577380
5	Very high	Very high	0.9258201	1.5583874
6	High	Medium	1.0000000	1.6832508
7	High	Medium	1.0000000	1.6124515
8	Very high	High	1.0000000	1.5000000
9	Very high	Very high	1.1547005	1.6329932
10	Medium	Medium	1.4142136	2.0000000
11	Very high	Medium	0.0000000	2.0000000
Average			0.9029218	1.5922666

4. Conclusions

Elevation products such as DTM and DEMNAS effectively map landslides. Differences in spatial resolution between DTM and DEMNAS result in varying landslide area estimations, although the landslide patterns are generally similar. Processed variables from DTM and DEMNAS, including aspect, curvature, slope, drainage density, lineament density, and topographic wetness index, yield distinct values.

Zones of very high landslide susceptibility are predominantly located in the western and eastern areas, characterized by very steep slopes, high drainage density, high lineament density, and several rock outcrops, which are indicative of fault lines. Landslide susceptibility is classified into five categories: very high, high, medium, low, and very low. While the overall area proportions are comparable, significant differences are observed in the "very low," "low," and "medium" categories.

DTM provides more detailed results, producing more significant values, whereas DEMNAS offers more generalized data. The RMSE values indicate that the DTM product, with an RMSE of 0.902 (derived from UAV data acquisition), has better accuracy in landslide mapping compared to DEMNAS, which has an RMSE of 1.592. Both products are effective for mapping landslides in the Lembang Fault area, as they exhibit good RMSE values for analysis.

The comparative study effectively validates the superiority of high-resolution UAV-derived DTMs over national-scale DEMNAS for landslide mapping along the Lembang Fault, as evidenced by a strong RMSE of 0.902, while correctly leveraging relevant geomorphological proxies for fault lines. However, the noted discrepancies in the "very low" to "medium" susceptibility categories likely stem from the DTM capturing micro-topographic noise in gentler terrains, whereas DEMNAS heavily smooths these features out.

To improve classification reliability in these lower-risk zones, this research recommends applying low-pass smoothing filters to the DTM and using multi-directional flow algorithms for the Topographic Wetness Index (TWI) to reduce erratic, localized data. Furthermore, integrating non-topographic variables, such as land use, vegetation, and soil depth, alongside advanced Machine Learning algorithms like Random Forest can better handle the complex, non-linear data in moderate terrains, ultimately harmonizing the differing resolutions into a more accurate and unified susceptibility model.

References

Abduh, A. G., Usman, F. C. A., Tampoy, W. M., & Manyoe, I. N. (2021). Remote sensing analysis of lineaments using multi-directional shaded relief from digital elevation model (DEM) in Olele area, Gorontalo. *Journal of Physics*: *Conference Series*, *1783*, Article 012095. IOP Publishing. https://doi.org/10.1088/1742-6596/1783/1/012095

Arrasyid, R., Ihsan, H. M., Ruhimat, M., & Pratama, A. R. (2023). Suitability evaluation of land use/land cover (LULC) towards landslide prone areas in structural and volcano landform. *International Journal of Geoinformatics*, *19*(6), 61–75.

Artese, S., & Perrelli, M. (2018). Monitoring a landslide with high accuracy by total station: A DTM-based model to correct for the atmospheric effects. *Geosciences*, *8*(2), Article 46. https://doi.org/10.3390/geosciences8020046

Capitani, M., Ribolini, A., & Bini, M. (2013). The slope aspect: A predisposing factor for landsliding?. *Comptes Rendus. Geoscience*, *345*(11–12), 427–438. https://doi.org/10.1016/j.crte.2013.11.002

Çellek, S. (2020). Effect of the slope angle and its classification on landslide. *Natural Hazards and Earth System Sciences Discussions* [preprint]. https://doi.org/10.5194/nhess-2020-87

Chauhan, S., Sharma, M., Arora, M. K., & Gupta, N. K. (2010). Landslide susceptibility zonation through ratings derived from artificial neural network. *International Journal of Applied Earth Observation and Geoinformation*, *12*(5), 340–350. https://doi.org/10.1016/j.jag.2010.04.006

Conforti, M., Mercuri, M., & Borrelli, L. (2020). Morphological changes detection of a large earthflow using archived images, LiDAR-derived DTM, and UAV-based remote sensing. *Remote Sensing*, *13*(1), Article 120. https://doi.org/10.3390/rs13010120

Daryono, M. R., Natawidjaja, D. H., Sapiie, B., & Cummins, P. (2019). Earthquake geology of the Lembang Fault, West Java, Indonesia. *Tectonophysics*, *751*, 180–191. https://doi.org/10.1016/j.tecto.2018.12.014

Eker, R., Aydın, A., & Hübl, J. (2018). Unmanned aerial vehicle (UAV)-based monitoring of a landslide: Gallenzerkogel landslide (Ybbs-Lower Austria) case study. *Environmental Monitoring and Assessment*, *190*, Article 28. https://doi.org/10.1007/s10661-017-6402-8

Gorokhovich, Y., & Vustianiuk, A. (2021). Implications of slope aspect for landslide risk assessment: A case study of Hurricane Maria in Puerto Rico in 2017. *Geomorphology*, *391*, Article 107874. https://doi.org/10.1016/j.geomorph.2021.107874

He, R., Zhang, W., Dou, J., Jiang, N., Xiao, H., & Zhou, J. (2024). Application of artificial intelligence in three aspects of landslide risk assessment: A comprehensive review. *Rock Mechanics Bulletin*, *3*(4), Article 100144. https://doi.org/10.1016/j.rockmb.2024.100144

Henriques, C., Zêzere, J. L., & Marques, F. (2015). The role of the lithological setting on the landslide pattern and distribution. *Engineering Geology*, *189*, 17–31. https://doi.org/10.1016/j.enggeo.2015.01.025

Hussin, H., Fauzi, A., Ghani, M. F. A., & Jaya, A. (2022). An approach to find the potential landslide source based on intersection of lineament using SRTM DEM. *AIP Conference Proceedings*, *2454*(1), Article 050023. AIP Publishing. https://doi.org/10.1063/5.0078941

Horton, R. E. (1932). Drainage basin characteristics. *Eos*, *Transactions American Geophysical Union*, *13*(1), 350–361. https://doi.org/10.1029/TR013i001p00350

Intrieri, E., Carlà, T., & Gigli, G. (2019). Forecasting the time of failure of landslides at slope-scale: A literature review. *Earth-Science Reviews*, *193*, 333–349. https://doi.org/10.1016/j.earscirev.2019.03.019

Jancewicz, K., Migoń, P., & Kasprzak, M. (2019). Connectivity patterns in contrasting types of tableland sandstone relief revealed by Topographic Wetness Index. *Science of the Total Environment*, *656*, 1046–1062. https://doi.org/10.1016/j.scitotenv.2018.11.467

Li, Y., & Mo, P. (2019). A unified landslide classification system for loess slopes: A critical review. *Geomorphology*, *340*, 67–83. https://doi.org/10.1016/j.geomorph.2019.04.020

Lindner, G., Schraml, K., Mansberger, R., & Hübl, J. (2016). UAV monitoring and documentation of a large landslide. *Applied Geomatics*, *8*, 1–11. https://doi.org/10.1007/s12518-015-0165-0

Mathew, J., Jha, V. K., & Rawat, G. S. (2007). Weights of evidence modelling for lansdslide hazard zonation mapping in part of Bhagirathi valley, Uttarakhand. *Current Science*, *92*, 628–638.

Meneses, B. M., Pereira, S., & Reis, E. (2019). Effects of different land use and land cover data on the landslide susceptibility zonation of road networks. *Natural Hazards and Earth System Sciences*, *19*(3), 471–487. https://doi.org/10.5194/nhess-19-471-2019

Neamat, S., & Karimi, H. (2020, December 23–24). A systematic review of GIS-based landslide Hazard mapping on determinant factors from international databases. In *Proceedings of the 2020 International Conference on Advanced Science and Engineering* (*ICOASE*) (pp. 180–183). Duhok, Iraq. IEEE. https://doi.org/10.1109/ICOASE51841.2020.9436611

Pawłuszek, K., Marczak, S., Borkowski, A., & Tarolli, P. (2019). Multi-aspect analysis of object-oriented landslide detection based on an extended set of LiDAR-derived terrain features. *ISPRS International Journal of Geo-Information*, *8*(8), Article 321. https://doi.org/10.3390/ijgi8080321

Pradhan, A. M. S., & Kim, Y. T. (2018). GIS-based landslide susceptibility model considering effective contributing area for drainage time. *Geocarto International*, *33*(8), 810–829. https://doi.org/10.1080/10106049.2017.1303089

Qiu, H., Zhu, Y., Zhou, W., Sun, H., He, J., & Liu, Z. (2022). Influence of DEM resolution on landslide simulation performance based on the Scoops3D model. *Geomatics*, *Natural Hazards and Risk*, *13*(1), 1663–1681. https://doi.org/10.1080/19475705.2022.2097451

Rai, P. K., Mohan, K., & Kumra, V. K. (2014). Landslide hazard and its mapping using remote sensing and GIS. *Journal of Scientific Research*, *58*(1), 1–13.

Ran, Q., Hong, Y., Li, W., & Gao, J. (2018). A modelling study of rainfall-induced shallow landslide mechanisms under different rainfall characteristics. *Journal of Hydrology*, *563*, 790–801. https://doi.org/10.1016/j.jhydrol.2018.06.040

Rasmid, R. (2014). Aktivitas Sesar Lembang di Utara Cekungan Bandung [Lembang Fault activity in the north of the Bandung Basin]. *Jurnal Meteorologi dan Geofisika*, *15*(2). https://doi.org/10.31172/jmg.v15i2.182

Ricky, N. K., & Basyid, M. A. (2021). Pemetaan potensi kerawanan bencana gempa bumi akibat sesar Lembang di Kawasan Kabupaten Bandung Barat [Mapping potential vulnerability to earthquake disasters due to the Lembang Fault in the west Bandung Regency Agency]. In *FTSP Series 2*: *Seminar Nasional dan Diseminasi Tugas Akhir* (pp. 563–576). Penerbit Itenas.

Roccati, A., Paliaga, G., Luino, F., Faccini, F., & Turconi, L. (2021). GIS-based landslide susceptibility mapping for land use planning and risk assessment. *Land*, *10*(2), Article 162. https://doi.org/10.3390/land10020162

Roda-Boluda, D. C., D'Arcy, M., McDonald, J., & Whittaker, A. C. (2018). Lithological controls on hillslope sediment supply: insights from landslide activity and grain size distributions. *Earth Surface Processes and Landforms*, *43*(5), 956–977. https://doi.org/10.1002/esp.4281

Różycka, M., Migoń, P., & Michniewicz, A. (2017). Topographic Wetness Index and Terrain Ruggedness Index in geomorphic characterisation of landslide terrains, on examples from the Sudetes, SW Poland. *Zeitschrift für Geomorphologie*, *61*(2), 61–80. https://doi.org/10.1127/zfg_suppl/2016/0328

Sadiq, S., Muhammad, U., & Fuchs, M. (2022). Investigation of landslides with natural lineaments derived from integrated manual and automatic techniques applied on geospatial data. *Natural Hazards*, *110*, 2141–2162. https://doi.org/10.1007/s11069-021-05028-6

Saleem, N., Huq, M. E., Twumasi, N. Y. D., Javed, A., & Sajjad, A. (2019). Parameters derived from and/or used with digital elevation models (DEMs) for landslide susceptibility mapping and landslide risk assessment: A review. *ISPRS International Journal of Geo-Information*, *8*(12), Article 545. https://doi.org/10.3390/ijgi8120545

Samia, J., Temme, A., Bregt, A., Wallinga, J., Guzzetti, F., Ardizzone, F., & Rossi, M. (2017). Characterization and quantification of path dependency in landslide susceptibility. *Geomorphology*, *292*, 16–24. https://doi.org/10.1016/j.geomorph.2017.04.039

Segoni, S., Piciullo, L., & Gariano, S. L. (2018). A review of the recent literature on rainfall thresholds for landslide occurrence. *Landslides*, *15*(8), 1483–1501. https://doi.org/10.1007/s10346-018-0966-4

Shao, X., & Xu, C. (2022). Earthquake-induced landslides susceptibility assessment: A review of the state-of-the-art. *Natural Hazards Research*, *2*(3), 172–182. https://doi.org/10.1016/j.nhres.2022.03.002

Sujit, M. (2015). Upslope contributing area, topographic wetness and landsliding: A case STUDY of the Shivkhola Watershed, Darjiling Himalaya. *International Research Journal of Earth Sciences*, *3*(7), 2321–2527.

Sulaiman, M. S., Nazaruddin, A., Salleh, N. M., Abidin, R. Z., Miniandi, N. D., & Yusoff, A. H. (2019). Landslide occurrences in Malaysia based on soil series and lithology factors. *International Journal of Advanced Science and Technology*, *28*(18), 1–26.

Sun, J., Yuan, G., Song, L., & Zhang, H. (2024). Unmanned aerial vehicles (UAVs) in landslide investigation and monitoring: A review. *Drones*, *8*(1), Article 30. https://doi.org/10.3390/drones8010030

Sun, X., Chen, J., Han, X., Bao, Y., Zhou, X., & Peng, W. (2020). Landslide susceptibility mapping along the upper Jinsha River, south-western China: A comparison of hydrological and curvature watershed methods for slope unit classification. *Bulletin of Engineering Geology and the Environment*, *79*, 4657–4670. https://doi.org/10.1007/s10064-020-01849-0

Tjahjadi, M. E., Maulinda, Noraini, A., Arafah, F., Jasmani & Dwi, F. (2020). Pemanfaatan DEMNAS untuk Menentukan Tinggi Terbang UAV Terhadap Permukaan Tanah [Use of DEMNAS (National digital elevation model) to determine the flying height of the UAV against the ground surface]. In *Prosiding Semsina 2020* (pp. PAR-III-29–PAR-III-32). Institut Teknologi Nasional Malang.

Ya'acob, N., Rahman, A. A. A., Yusof, A. L., Ali, D. M., & Naim, N. F. (2024). Landslide detection using analysed UAV imagery. *Journal of Advanced Research in Applied Sciences and Engineering Technology*, *45*(1), 168–188. https://doi.org/10.37934/araset.45.1.168188

Zhao, T., Dai, F., & Xu, N.-W. (2017). Coupled DEM-CFD investigation on the formation of landslide dams in narrow rivers. *Landslides*, *14*, 189–201. https://doi.org/10.1007/s10346-015-0675-1

Zhou, J., Jiang, N., Li, C., & Li, H. (2023). A landslide monitoring method using data from unmanned aerial vehicle and terrestrial laser scanning with insufficient and inaccurate ground control points. *Journal of Rock Mechanics and Geotechnical Engineering*, *16*(10), 4125–4140. https://doi.org/10.1016/j.jrmge.2023.12.004

Zou, Q., Jiang, H., Cui, P., Zhou, B., Jiang, Y., Qin, M., Liu, Y., & Li, C. (2021). A new approach to assess landslide susceptibility based on slope failure mechanisms. *Catena*, *204*, Article 105388. https://doi.org/10.1016/j.catena.2021.105388